Polymer Chemistry

PAPER

View Article Online
View Journal | View Issue

Cite this: *Polym. Chem.*, 2016, **7**, 6375

Synthesis and multimodal responsiveness of poly(α-amino acid)s bearing OEGylated azobenzene side-chains†

Wei Xiong,[a] Xiaohui Fu,[b] Yaoming Wan,[c] Yunlong Sun,[a] Zhibo Li*[b] and Hua Lu*[a]

Received 4th August 2016,
Accepted 23rd September 2016

DOI: 10.1039/c6py01364c

www.rsc.org/polymers

Stimuli-responsive poly(α-amino acids) (PαAAs) are protein mimics that can alter their conformational or other physicochemical properties in response to external triggers. We report here the synthesis and characterization of novel photo and thermal responsive PαAAs by the ring-opening polymerization of α-amino acid *N*-carboxyanhydrides (NCAs). Specifically, a series of NCA monomers bearing azobenzene (Azo) and oligoethylene glycol (OEG) of different lengths (OEG_m-AzoNCA, m = 2, 4, 6) are synthesized in a modular route and polymerized in a controlled manner using hexamethyldisilazane (HMDS) as the initiator. The afforded $P(OEG_m\text{-Azo})_n$s show interesting aggregation behaviors in both organic and aqueous solutions. Moreover, $P(OEG_m\text{-Azo})_n$s exhibit a reversible photo-responsiveness accompanied by the conformational switch of the peptidic backbone, and an irreversible thermal-responsiveness. This new biodegradable and stimuli-responsive system holds considerable promise for applications such as on-demand delivery, liquid crystalline, and hierarchical self-assembly.

1. Introduction

Stimuli-responsive polymers are smart materials that can change their physical or/and chemical properties (*e.g.* primary structures or solubility) by means of external triggers.[1,2] More attractively, stimuli-responsive poly(α-amino acid)s (PαAAs) can show additional merits such as switching of conformational structures between a disordered and an ordered state.[3,4] Along this direction, many stimuli-responsive (*e.g.* pH, temperature, light, redox, biomolecules) PαAAs have been realized by the ring-opening polymerization (ROP) of α-amino acid *N*-carboxyanhydrides (NCAs) or post-modification of functional PαAAs, and hold substantial promise for various applications.[4–14] Moreover, several multimodal responsive PαAAs have been elegantly demonstrated.[15–23] For instance, Kramer and Deming reported redox and thermal responsive poly(*S*-alkyl-L-homocysteine)s which showed reversible switching in water solubility and chain conformation.[17] Dong *et al.* recently designed a photo and redox responsive PEG-poly(*S*-(*o*-nitrobenzyl)-L-cysteine) block copolymer that self-assembled into vesicles and then could be converted to micelles upon applying triggers.[15] Li and coworkers described poly(L-cysteine) modified by oligoethylene glycol (OEG) *via* the disulfide bond, which showed irreversible LCST and redox behaviors.[18]

Among all triggers explored, light is particularly attractive for its noninvasive nature and precise spatio-temporal control. Frequently, a photo sensitive or labile moiety (*e.g.* *o*-nitrobenzyl,[24–26] azobenzene (Azo),[27–37] or spiropyran[38]) is incorporated to the side-chain of PαAAs to impart responsiveness to light. Particularly, Azo is a broadly exploited photosensitive segment introduced to the side-chain of poly(L-lysine),[30,32] poly(L-glutamate),[27] and poly(L-phenylalanine)[28] through post-polymerization modification or ROP of Azo-bearing monomers. However, due to the structural rigidity and strong π–π interactions, the resulting Azo-bearing PαAAs often suffer from poor solubility, particularly in water, and are thus commonly studied in the form of random copolymers together with other polypeptides for the sake of better solubility. Most frequently, the contents of Azo in these polymers are reported to be less than 50%; as a result, their photo-responsiveness usually produces a less prominent effect than polymers with higher Azo contents.[39] To study the properties of homo PαAAs with Azo side-chains, we seek to design and synthesize NCAs bearing amphiphilic OEGylated Azo side chains

[a]*Beijing National Laboratory for Molecular Sciences, Center for Soft Matter Science and Engineering, Key Laboratory of Polymer Chemistry and Physics of Ministry of Education, College of Chemistry and Molecular Engineering, Peking University, Beijing 100871, China. E-mail: chemhualu@pku.edu.cn*
[b]*School of Polymer Science and Engineering, Qingdao University of Science and Technology, Qingdao 266042, China. E-mail: zbli@qust.edu.cn*
[c]*Beijing National Laboratory for Molecular Sciences, Laboratory of Polymer Physics and Chemistry, Institute of Chemistry, Chinese Academy of Sciences, Beijing 100190, China*

†Electronic supplementary information (ESI) available. See DOI: 10.1039/c6py01364c

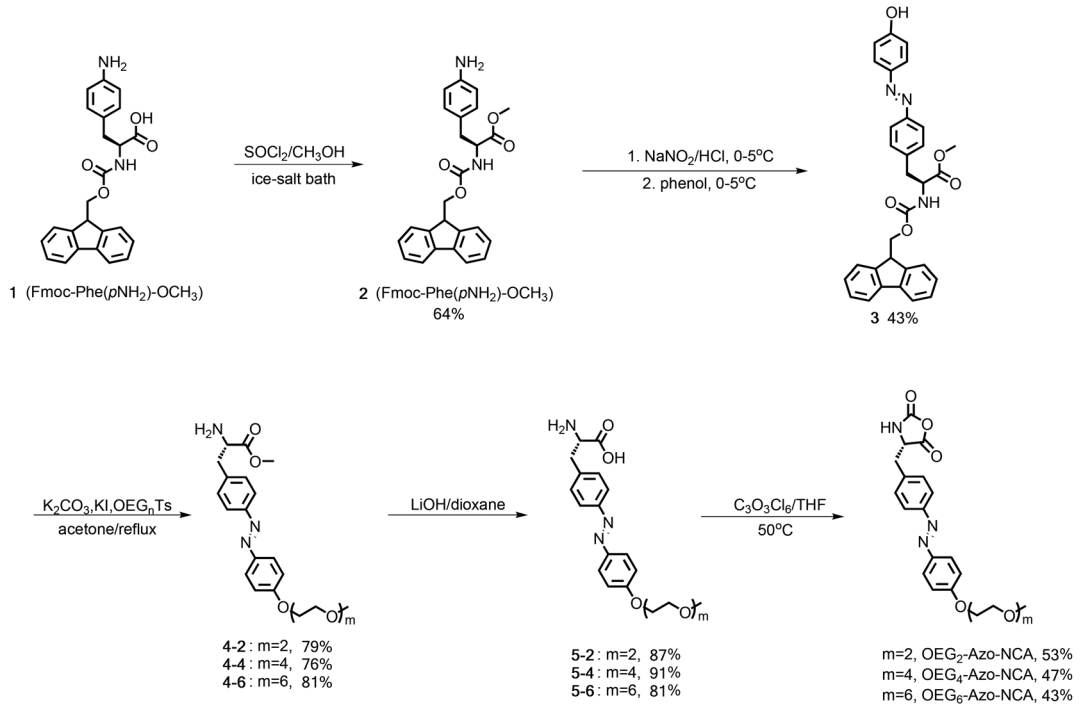

Scheme 1 Synthesis of OEG_m-AzoNCA (m = 2, 4, or 6).

(OEG_m-AzoNCAs, Scheme 1). Here, OEG units are introduced to improve sample solubility in various solvents, and to offer potential thermal-responsiveness in water.[40,41] Altogether, we believe that the OEG- and Azo-bearing PαAAs designed in this work are worth pursuing for their interesting aggregation, self-assembly, and multimodal responsiveness behaviors, and are potential candidates for a variety biological applications.

2. Results and discussion

2.1 Synthesis of OEG_m-AzoNCAs

A series of Azo- and OEG-bearing NCAs were synthesized in an efficient and modular route, as shown in Scheme 1. Briefly, we began the synthesis by protecting the carboxylic acid of Fmoc-Phe($p$$NH_2$)-OH (**1**) to yield Fmoc-Phe($p$$NH_2$)-OMe (**2**), which was then converted to **3** by firstly transforming the side-chain amine of **2** to diazonium salt and followed by treatment with phenol. The Azo-installed **3** was used as a universal precursor for all NCA monomers reported here. Upon deprotonation of the phenol hydroxyl of **3** with potassium carbonate, the nucleophilic phenoxide salt efficiently attacked tosylated OEGs of various lengths (OEG_mOTs, m = 2, 4, and 6) to generate the desired ether bond. Interestingly and unexpectedly, the Fmoc group was also removed to afford a series of compounds **4-*m*** (m = 2, 4, and 6) during the OEGylation step. The yields of **4-*m*** were ~76–81%, which implied that this integrated OEGylation and deprotection reaction was relatively clean and robust. After hydrolysis of the methyl ester by using lithium hydroxide to afford **5-*m*** (m = 2, 4, and 6), three OEG_m-AzoNCAs (m = 2, 4, and 6) were obtained by cyclization of **5-*m*** in dry THF with triphosgene. All precursors and NCAs were comprehensively characterized by mass spectrometry, FT-IR, ^{1}H and ^{13}C NMR spectroscopy, which are compiled in Fig. S1–S11.† Taking OEG_6-AzoNCA as an example, the formation of NCAs was confirmed by the characteristic N–H proton at ~9.1 ppm in DMSO-d_6 (Fig. 1). The monomers were considerably stable under ambient conditions, as they can be easily purified by regular column chromatography and the shelf-lives of these monomers were up to 3–4 weeks outside the glove box.

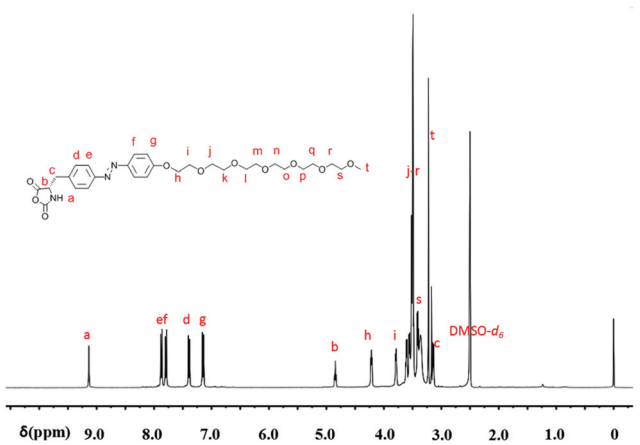

Fig. 1 ^{1}H NMR spectrum of OEG_6-AzoNCA in DMSO-d_6.

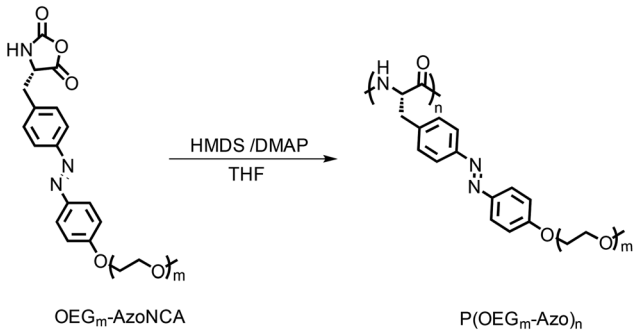

Scheme 2 Synthesis of P(OEG$_m$-Azo)$_n$.

2.2 ROP of OEG$_m$-AzoNCAs and aggregation of P(OEG$_m$-Azo)$_n$s

Next, we employed hexamethyldisilazane (HMDS, initiator, 1.0 equiv.) and *N*,*N*-dimethylaminopyridine (DMAP, catalyst, 0.3 equiv.) to mediate the ROP of OEG$_m$-AzoNCAs in THF (Scheme 2).[42,43] After the monomers were consumed as measured by FT-IR spectroscopy, the polymers termed P(OEG$_m$-Azo)$_n$s (m = 2, 4, or 6; n = feeding monomer/initiator ratios) were precipitated and washed with diethyl ether, and dried under vacuum (^{1}H NMR spectra in Fig. S12–S14†). Due to the presence of OEG$_m$, all P(OEG$_m$-Azo)$_n$s displayed remarkably good solubility in common organic solvents such as DMF, THF, dichloromethane, and even methanol. In aqueous buffers, only P(OEG$_6$-Azo)$_n$s, those with the longest OEG side chain, showed observable solubility in a fashion depending on the degree of polymerization (DP). Despite their good apparent solubility, several pieces of evidence suggested that P(OEG$_m$-Azo)$_n$s actually existed as nano-sized aggregates in many solvents. For instance, a strong dynamic light scattering (DLS) signal was observed in P(OEG$_6$-Azo)$_{50}$ methanol solution (Fig. 2A). Transmission electron microscopy (TEM) also showed nanoscale particles for the P(OEG$_6$-Azo)$_{50}$ solution in water (Fig. 2B). The Nile Red encapsulation assay in water depicted a critical micelle concentration (CMC) value of ~0.15 mg mL^{-1} for P(OEG$_6$-Azo)$_{50}$ (Fig. 2C). Moreover, we observed a typical aggregation-induced emission (AIE)[44,45] phenomenon in these polymers, which further implied the above described aggregation behaviors. Briefly, as shown in Fig. 2D, when a solution of P(OEG$_6$-Azo)$_{50}$ in THF was titrated with ultrapure water, a striking increase (~18 fold) of fluorescence intensity at ~516 nm was observed when the water/THF (v/v) ratio reached 9/1. Presumably, we attributed the dispersibility of P(OEG$_6$-Azo)$_n$ to OEG$_6$, and the strong

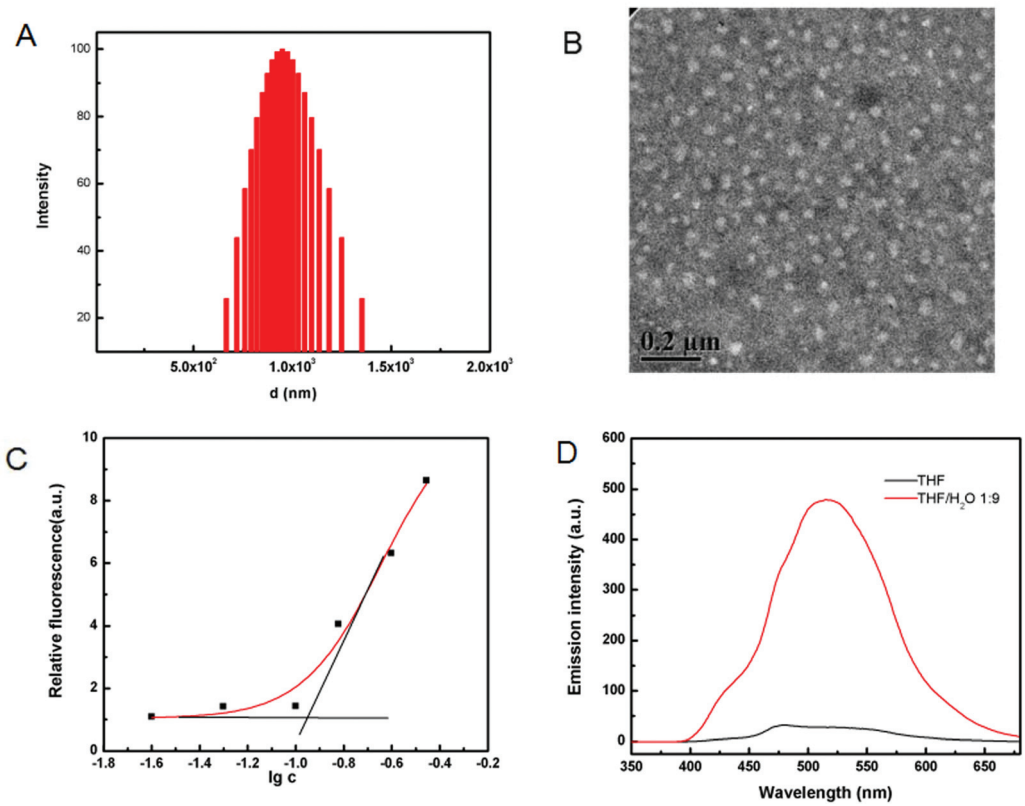

Fig. 2 Aggregation of P(OEG$_6$-Azo)$_{50}$. (A) DLS measurement of P(OEG$_6$-Azo)$_{50}$ in methanol (c = 0.1 mg mL^{-1}). (B) TEM of P(OEG$_6$-Azo)$_{50}$ in H$_2$O (c = 0.5 mg mL^{-1}); the sample was negatively stained by using uranyl acetate. (C) Measurement of the critical micelle concentration of P(OEG$_6$-Azo)$_{50}$ in H$_2$O by Nile Red encapsulation assay. (D) Fluorescence spectra of P(OEG$_6$-Azo)$_{50}$ in different solvents (c = 0.4 mg mL^{-1}); excitation wavelength = 233 nm.

Table 1 High temperature GPC characterization of P(OEG$_m$-Azo)$_n$s

Entry	Polymers	M/I	M_n exp.[a] (g mol^{-1})	M_n obt.[b] (g mol^{-1})	PDI[c] (M_w/M_n)
1	P(OEG$_2$-Azo)$_{10}$	10	3690	3488	1.03
2	P(OEG$_2$-Azo)$_{50}$	50	18 450	18 044	1.19
3	P(OEG$_4$-Azo)$_{10}$	10	4570	4351	1.05
4	P(OEG$_4$-Azo)$_{50}$	50	22 850	17 697	1.15
5	P(OEG$_6$-Azo)$_{10}$	10	5450	4564	1.07
6	P(OEG$_6$-Azo)$_{50}$	50	27 250	20 006	1.29

[a] M_n exp. = expected molecular weight (feeding M/I ratio). [b] M_n obt. = obtained molecular weight. [c] PDI = polydispersity index, determined by GPC.

aggregation of P(OEG$_6$-Azo)$_n$ was likely a combined result of the intermolecular hydrogen bonding of the peptide backbone and the π–π stacking of the Azo segment. The DLS data of other P(OEG$_m$-Azo)$_n$s are shown in Table S1.†

Accordingly, we noticed that tandem gel permeation chromatography (GPC) analysis of P(OEG$_m$-Azo)$_n$s in DMF with 0.1 M LiBr at 60 °C, a routinely used condition for PαAA characterization, also gave peaks belonging to the aggregates (data not shown). After screening of GPC conditions, we finally obtained the molecular weight (MW) and the polydispersity index (PDI) of P(OEG$_m$-Azo)$_n$s with high-temperature GPC in 1,2,4-trichlorobenzene at 150 °C (Table 1 and Fig. 3). All polymers showed monomodal peaks, good MW control with small deviation from the expected values, and acceptable narrow PDIs, indicating that the polymerizations were executed in a well-controlled manner.

2.3 Photo-responsiveness of P(OEG$_m$-Azo)$_n$s

To demonstrate the photo-responsiveness of P(OEG$_m$-Azo)$_n$s, both OEG$_6$-AzoNCA and P(OEG$_6$-Azo)$_{10}$ were exposed to UV irradiation (lamp power 30 W, wavelength of 365 nm) and examined by ^{1}H NMR spectroscopy. As expected, OEG$_6$-AzoNCA displayed a remarkable shift of the Azo peaks after the treatment (Fig. S15†). Similarly, a rapid shift from 7.8–7.6 ppm to 6.9–6.7 ppm that corresponded to the photo-triggered *trans–cis* transition was observed for P(OEG$_6$-Azo)$_{10}$ after UV exposure, as shown in Fig. 4A and B. A ~82% and ~54% *trans–cis* transition was calculated for OEG$_6$-AzoNCA and P(OEG$_6$-Azo)$_{10}$, respectively. Prolonging the irradiation process, however, did not increase the relative ratios of the *cis*-isomers for both NCAs and polymers. Increasing the power of the UV lamp to 400 W accelerated the isomerization rate significantly, but the reaction equilibria (conversion yields) were only marginally affected for both OEG$_6$-AzoNCA and P(OEG$_6$-Azo)$_{10}$ (~86% and ~66%, respectively, Fig. S16†). Moreover, UV-Vis spectroscopy of P(OEG$_6$-Azo)$_{10}$ before and after UV irradiation depicted a characteristic two-state process attributable to the same *trans–cis* transition of Azo (Fig. 4C). Briefly, the initial P(OEG$_6$-Azo)$_{10}$ in the *trans*-conformation showed a strong Azo absorption peak at ~329 nm associated with a π–π* transition, which decreased dramatically upon UV-irradiation. Concurrently, a small peak emerged at ~430 nm associated with an n–π* transition for the newly formed *cis*-P(OEG$_6$-Azo)$_{10}$. Two isosbestic points appeared in the UV-Vis spectrum at ~282 and 400 nm, respectively. It is worth noting that the solubility of *cis*-P(OEG$_6$-Azo)$_n$s in water was greatly improved as compared to their *trans* isomers, a phenomenon frequently observed in other Azo-bearing systems, to which we attributed the increased polarity of the *cis*-Azo moiety (Fig. S17†).[39] Indeed, DLS examination of *cis*-P(OEG$_6$-Azo)$_n$s (n = 10 and 50) in water did not show a measurable signal. This result was also confirmed by the Nile Red encapsulation assay as no definite CMC value was determined for *cis*-P(OEG$_6$-Azo)$_{50}$. To demonstrate the photo-reversibility, the UV-treated OEG$_6$-AzoNCA and P(OEG$_6$-Azo)$_{10}$ were subjected to visible light irradiation (lamp power 275 W). Both monomer and polymer showed a rapid *cis–trans* isomerization as shown in Fig. S15† and Fig. 4B, C.

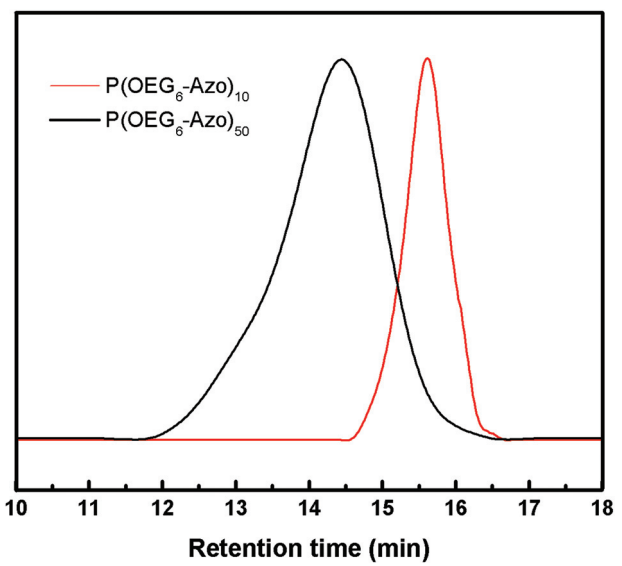

Fig. 3 Overlay of GPC curves of P(OEG$_6$-Azo)$_n$s (n = 10, red; n = 50, black).

2.4 Secondary conformation of P(OEG$_m$-Azo)$_n$s

Next, we studied the secondary structure of P(OEG$_6$-Azo)$_n$s by using circular dichroism (CD) spectroscopy. Before UV treatment, the peptidic backbone of *trans*-P(OEG$_6$-Azo)$_{10}$ exhibited a typical β-sheet structure in trifluoroethanol (TFE) with a minimum at ~216 nm in CD spectrum (Fig. 5A), whereas the

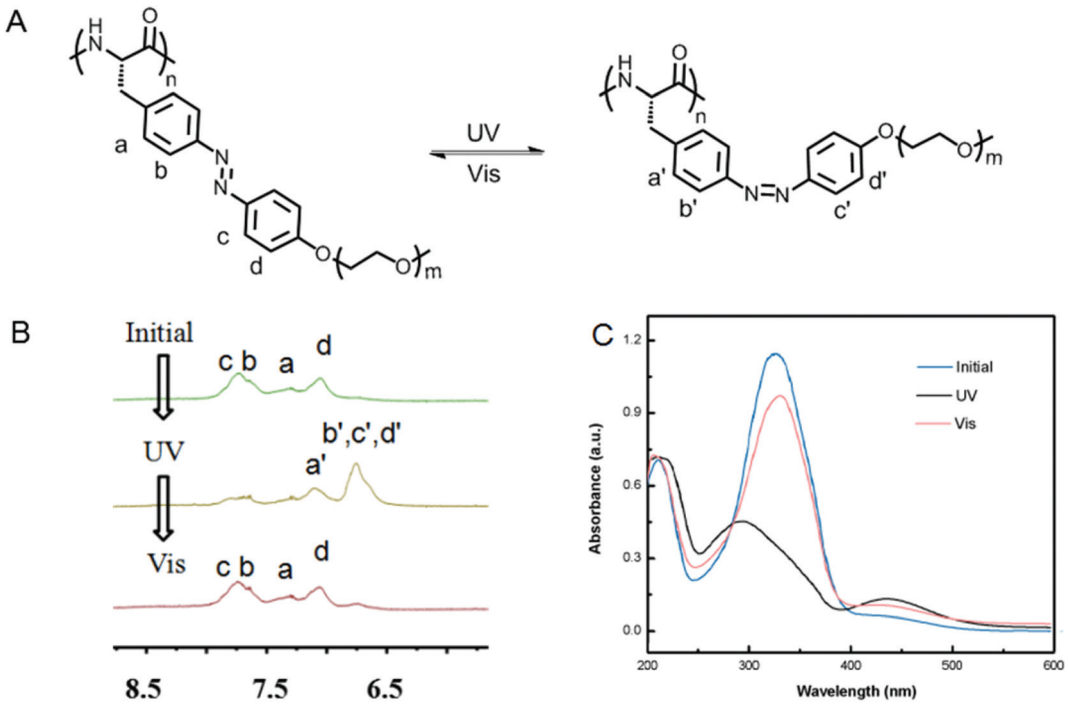

Fig. 4 Photo-responsiveness of P(OEG$_6$-Azo)$_{10}$. (A) Scheme of the UV-triggered *trans–cis* isomerization of P(OEG$_6$-Azo)$_{10}$. (B) ^{1}H NMR spectra of P(OEG$_6$-Azo)$_{10}$ in DMSO-d_6/TFA-d treated with UV (400 w, 365 nm) and Vis (275 w) irradiation. (C) UV-vis spectra of P(OEG$_6$-Azo)$_{10}$ solution (c = 0.1 mg mL^{-1}) treated with UV and Vis light.

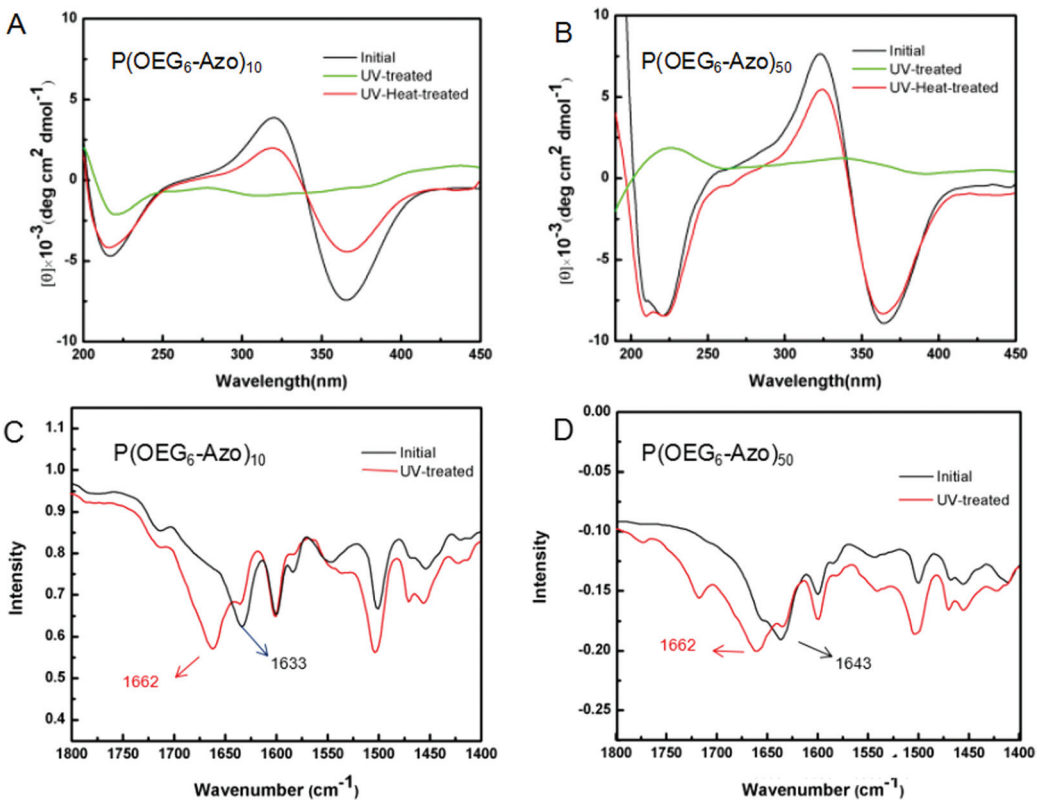

Fig. 5 Secondary structure of P(OEG$_6$-Azo)$_n$. (A, B) CD spectra of P(OEG$_6$-Azo)$_{10}$ (A) and P(OEG$_6$-Azo)$_{50}$ (B) in TFE; the polymers were first irradiated with UV at 365 nm for 5 min, followed by heating at 70 °C for 60 min. (C, D) FT-IR spectra of P(OEG$_6$-Azo)$_{10}$ (C) and P(OEG$_6$-Azo)$_{50}$ (D) in DCM.

higher-MW *trans*-P(OEG$_6$-Azo)$_{50}$ displayed a classical α-helical conformation evidenced by the double negative peaks at ~208 and 222 nm (Fig. 5B). Notably, both polymers showed the characteristic couplet of bands with opposite local maximum and minimum at 322 and 365 nm, respectively, which was in correspondence to the π–π* transition of the Azo component (Fig. 5A and B). The strong Azo signal in the CD spectra implied that the Azo group adopted an ordered conformation for both samples. Upon UV treatment, the initial CD patterns of both polymers disappeared (Fig. 5A and B), indicating the *trans–cis* isomerization of Azo in the side-chain forced *cis*-P(OEG$_6$-Azo)$_n$s to adopt a disordered conformation. Importantly, this conformational switch was reversible upon heating the UV-treated *cis*-polymers at 70 °C, as demonstrated by the recovered CD pattern (Fig. 5A and B). FT-IR spectroscopy of P(OEG$_6$-Azo)$_{10}$ and P(OEG$_6$-Azo)$_{50}$ further confirmed the CD results (Fig. 5C and D). Specifically, a characteristic amide I peak at ~1633 cm^{-1} attributed to the β-sheet structure was observed for P(OEG$_6$-Azo)$_{10}$ in DCM, which shifted to ~1662 cm^{-1} after UV exposure (Fig. 5C). Similarly, the shift of the amide I peak of P(OEG$_6$-Azo)$_{50}$ from ~1643 to ~1662 cm^{-1} after UV treatment indicated a change from a helix to a disordered structure (Fig. 5D). The secondary structures of P(OEG$_2$-Azo)$_n$s and P(OEG$_4$-Azo)$_n$s were also examined by FT-IR spectroscopy (Fig. S18–S21†).

2.5 Thermal responsiveness of P(OEG$_m$-Azo)$_n$s

OEG of different lengths are well-known to impart the lower critical solution temperature (LCST) property to the corresponding polymers, we therefore studied the thermal-responsiveness of P(OEG$_6$-Azo)$_n$s in water by measuring the transmittance at the wavelength of 500 nm. As shown in Fig. 6A, the aqueous solution of P(OEG$_6$-Azo)$_{10}$ became gradually turbid when the temperature was elevated at a rate of 1.0 °C min^{-1}. A relatively slow phase transition was recorded in the region from ~55 to 75 °C with a cloud point at ~62 °C. Upon UV irradiation, the resulting *cis*-P(OEG$_6$-Azo)$_{10}$ showed a gradual decrease in transmittance but did not reach any plateau up to ~98 °C, likely a consequence of the increased solubility of the *cis*-Azo isomer (Fig. 6A). In the cooling cycle, the transmittances of both *trans*- and *cis*-P(OEG$_6$-Azo)$_{10}$ did not follow their original heating curves but displayed a delayed recovery, suggesting that the larger aggregates generated at high temperatures cannot be dissociated in the cooling process. The thermal-responsiveness of P(OEG$_6$-Azo)$_{10}$ was also reflected by the temperature-dependent AIE effect, in which a ~13 fold fluorescence increase was detected at 85 °C as compared to its emission intensity at 35 °C (Fig. 6B). To understand the MW-dependence of thermal responsiveness, we performed the same study for P(OEG$_6$-Azo)$_{50}$. However, both *cis*- and *trans*-P(OEG$_6$-Azo)$_{50}$ precipitated in water at ~50 °C and the resulting suspensions could not redissolve in the cooling cycle (Fig. S22†), implying a stronger and irreversible aggregation.

2.6 Gel–sol transition for P(OEG$_m$-Azo)$_n$–PEG–P(OEG$_m$-Azo)$_n$ triblock copolymers

Because of the intense physical association and multimodal responsiveness of P(OEG$_m$-Azo)$_n$s, we sought to generate responsive gels based on P(OEG$_m$-Azo)$_n$s. For this purpose, a triblock copolymer P(OEG$_6$-Azo)$_7$–PEG–P(OEG$_6$-Azo)$_7$ was prepared by the ROP of OEG$_6$-AzoNCA using a bisamine-functionalized polyethylene glycol as the macro-initiator (NH_2-PEG-NH_2). The block copolymer was characterized by ^{1}H NMR and FT-IR spectroscopies (Fig. S23 and S24†). An organogel was generated by dissolving P(OEG$_6$-Azo)$_7$–PEG–P(OEG$_6$-Azo)$_7$ at a concentration of ~14 wt% in THF (Fig. 7A). The gel exhibited a rapid and reversible switch between a gel and a sol state upon Vis or UV treatment (Fig. 7A). The AFM images of the gel revealed a densely entangled fibrous network, which became less crosslinked after UV treatment (Fig. 7B and C). The same polymer, however, could not be dispersed in water, which was likely due to the crosslinking tendency of A–B–A type triblock copolymers when the A block has strong self-association. A similar gel–sol transition in THF was observed for another triblock polymer P(OEG$_4$-Azo)$_{10}$–PEG–P(OEG$_4$-Azo)$_{10}$ (Fig. S25†).

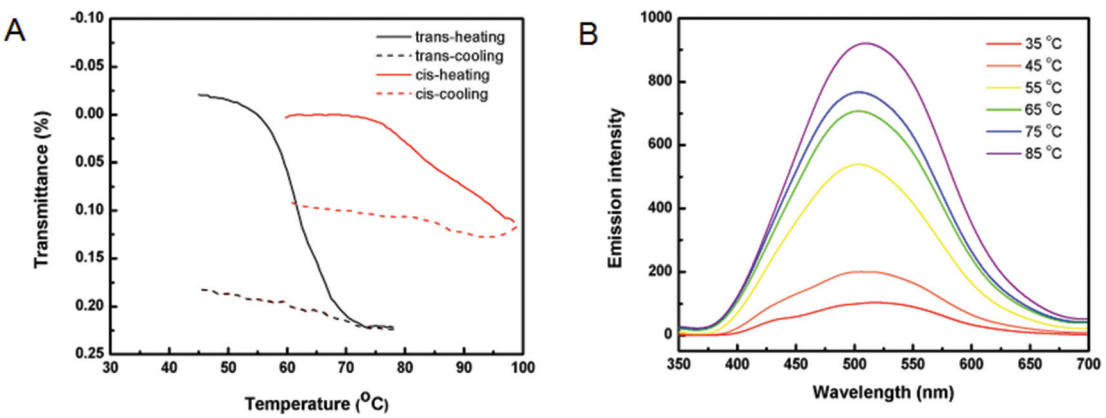

Fig. 6 Thermal-responsiveness of P(OEG$_6$-Azo)$_{10}$. (A) Temperature dependence of the transmittance at 500 nm of *trans*- and *cis*-P(OEG$_6$-Azo)$_{10}$ aqueous solutions (c = 0.2 mg mL^{-1}). (B) Fluorescence spectra of *trans*-P(OEG$_6$-Azo)$_{10}$ solution in water at different temperatures (c = 0.5 mg mL^{-1}).

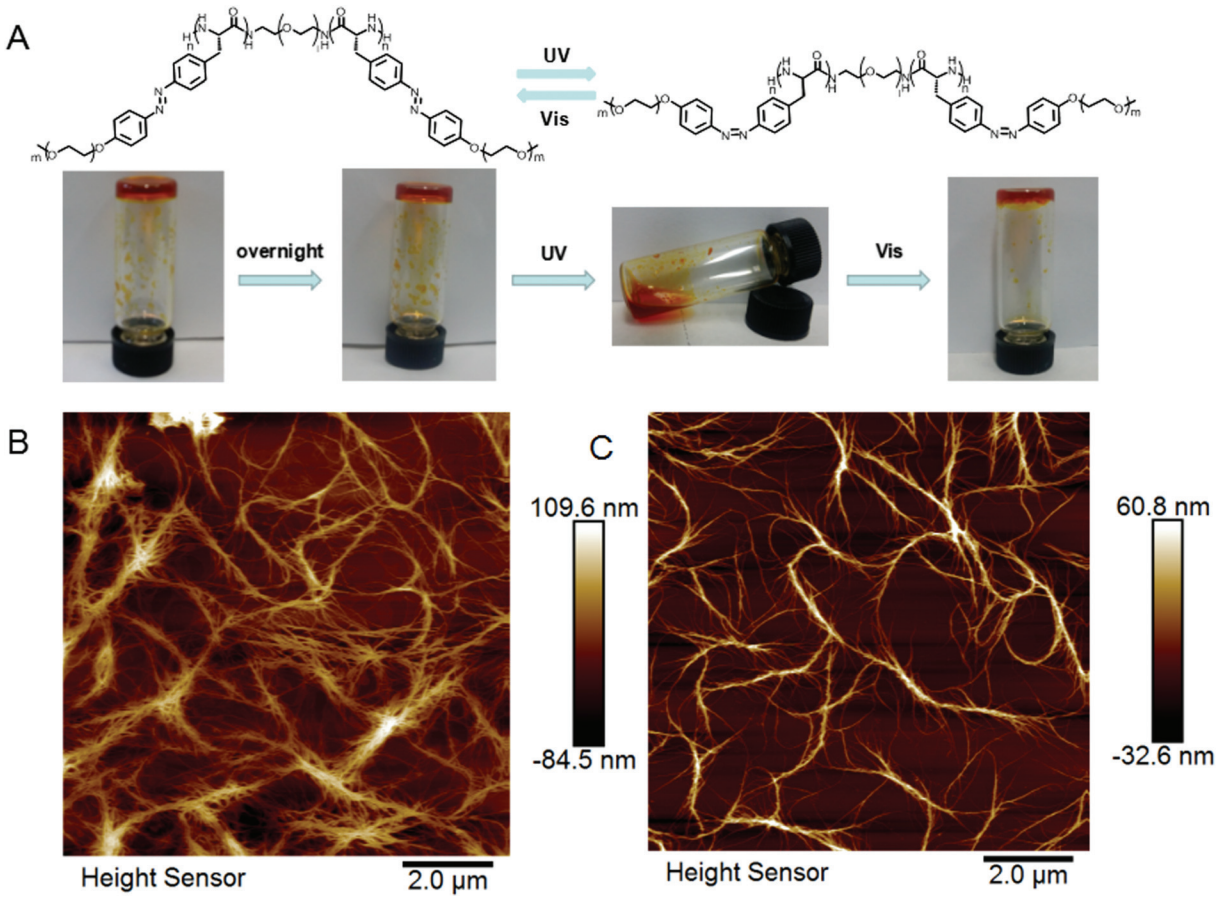

Fig. 7 (A) Photographs of the triblock co-polymer P(OEG$_6$-Azo)$_7$–PEG–P(OEG$_6$-Azo)$_7$ solution in THF showing the reversible UV-Vis triggered gel–sol transition. (B, C) AFM images of P(OEG$_6$-Azo)$_7$–PEG–P(OEG$_6$-Azo)$_7$ organogel in its original state (B) and after UV irradiation (C).

3. Conclusions

In conclusion, we described the tailored synthesis of three novel OEG$_m$-AzoNCA monomers bearing OEGylated Azo side-chains. The ROP of OEG$_m$-AzoNCAs resulted in a series of PαAAs with interesting aggregation behaviors in common organic and aqueous solutions. The secondary structure and multimodal responsiveness of P(OEG$_m$-Azo)$_n$s were carefully examined. Briefly, DP-dependent secondary structures (*e.g.* α-helices for higher DPs and β-sheet for lower DPs) of P(OEG$_m$-Azo)$_n$s were observed, which could be reversibly switched to a disordered conformation upon UV-Vis irradiation. Moreover, P(OEG$_6$-Azo)$_n$s displayed irreversible thermo-responsiveness in water. Photo-induced reversible gel–sol transition was demonstrated in a P(OEG$_6$-Azo)$_7$–PEG–P(OEG$_6$-Azo)$_7$ triblock copolymer system. Given the structural features and physicochemical properties demonstrated above, we believe that P(OEG$_m$-Azo)$_n$s are potentially promising building blocks for liquid crystalline, responsive organo- and hydrogels, hierarchical self-assembly, and drug delivery. Careful investigations of their phase transition in the solid state and liquid crystalline properties in bulk are currently underway in our laboratories, which will be separately reported in another work.

Acknowledgements

H. L. and Z. B. L. thank the grant from the National Natural Science Foundation of China (NSFC21434008). H. L. thanks the support from the Youth Thousand-Talents Program of China.

Notes and references

1 M. A. Stuart, W. T. Huck, J. Genzer, M. Muller, C. Ober, M. Stamm, G. B. Sukhorukov, I. Szleifer, V. V. Tsukruk, M. Urban, F. Winnik, S. Zauscher, I. Luzinov and S. Minko, *Nat. Mater.*, 2010, **9**, 101–113.
2 S. Mura, J. Nicolas and P. Couvreur, *Nat. Mater.*, 2013, **12**, 991–1003.
3 E. G. Bellomo, M. D. Wyrsta, L. Pakstis, D. J. Pochan and T. J. Deming, *Nat. Mater.*, 2004, **3**, 244–248.
4 K. S. Krannig, J. Sun and H. Schlaad, *Biomacromolecules*, 2014, **15**, 978–984.
5 J. Huang and A. Heise, *Chem. Soc. Rev.*, 2013, **42**, 7373–7390.

6 Y. Shen, X. Fu, W. Fu and Z. Li, *Chem. Soc. Rev.*, 2015, **44**, 612–622.
7 H. Lu, J. Wang, Z. Song, L. Yin, Y. Zhang, H. Tang, C. Tu, Y. Lin and J. Cheng, *Chem. Commun.*, 2014, **50**, 139–155.
8 F. Chécot, J. Rodríguez-Hernández, Y. Gnanou and S. Lecommandoux, *Polym. Adv. Technol.*, 2006, **17**, 782–785.
9 X. He, J. W. Fan and K. L. Wooley, *Chem. – Asian J.*, 2016, **11**, 437–447.
10 W. Tai, R. Mo, J. Di, V. Subramanian, X. Gu, J. B. Buse and Z. Gu, *Biomacromolecules*, 2014, **15**, 3495–3502.
11 C. He, X. Zhuang, Z. Tang, H. Tian and X. Chen, *Adv. Healthcare Mater.*, 2012, **1**, 48–78.
12 A. Kapetanakis and A. Heise, *Eur. Polym. J.*, 2015, **69**, 483–489.
13 S. S. Zhang, J. E. Burda, M. A. Anderson, Z. R. Zhao, Y. Ao, Y. Cheng, Y. Sun, T. J. Deming and M. V. Sofroniew, *ACS Biomater. Sci. Eng.*, 2015, **1**, 705–717.
14 S. S. Zhang, D. J. Alvarez, M. V. Sofroniew and T. J. Deming, *Biomacromolecules*, 2015, **16**, 1331–1340.
15 G. Liu, L. Z. Zhou, Y. F. Guan, Y. Su and C. M. Dong, *Macromol. Rapid Commun.*, 2014, **35**, 1673–1678.
16 C. H. Luo, Y. Liu and Z. B. Li, *Macromolecules*, 2010, **43**, 8101–8108.
17 J. R. Kramer and T. J. Deming, *J. Am. Chem. Soc.*, 2014, **136**, 5547–5550.
18 Y. N. Ma, X. H. Fu, Y. Shen, W. X. Fu and Z. B. Li, *Macromolecules*, 2014, **47**, 4684–4689.
19 H. Iatrou, H. Frielinghaus, S. Hanski, N. Ferderigos, J. Ruokolainen, O. Ikkala, D. Richter, J. Mays and N. Hadjichristidis, *Biomacromolecules*, 2007, **8**, 2173–2181.
20 J. Dai, S. D. Lin, D. Cheng, S. Y. Zou and X. T. Shuai, *Angew. Chem., Int. Ed.*, 2011, **50**, 9404–9408.
21 A. Zhang, J. G. Li, T. Wang, D. L. Wu, X. Q. Zhang, J. T. Yan, S. Du, Y. F. Guo and J. T. Wang, *Biomacromolecules*, 2008, **9**, 2670–2676.
22 C. X. Li, J. Adamcik, A. Zhang and R. Mezzenga, *Chem. Commun.*, 2011, **47**, 262–264.
23 W. Agut, A. Brulet, C. Schatz, D. Taton and S. Lecommandoux, *Langmuir*, 2010, **26**, 10546–10554.
24 G. Liu and C. M. Dong, *Biomacromolecules*, 2012, **13**, 1573–1583.
25 L. Yin, H. Tang, K. H. Kim, N. Zheng, Z. Song, N. P. Gabrielson, H. Lu and J. Cheng, *Angew. Chem., Int. Ed.*, 2013, **52**, 9182–9186.
26 J. R. Hernandez and H. A. Klok, *J. Polym. Sci., Part A: Polym. Chem.*, 2003, **41**, 1167–1187.
27 A. Fissi and O. Pieroni, *Macromolecules*, 1989, **22**, 1115–1120.
28 M. Sisido, Y. Ishikawa, K. Itoh and S. Tazuke, *Macromolecules*, 1991, **24**, 3993–3998.
29 M. Goodman and M. L. Falxa, *J. Am. Chem. Soc.*, 1967, **89**, 3863–3867.
30 H. Yamamoto, *Macromolecules*, 1986, **19**, 2472–2476.
31 H. Yamamoto, A. Nishida, T. Takimoto and A. Nagai, *J. Polym. Sci., Part A: Polym. Chem.*, 1990, **28**, 67–74.
32 A. Fissi, O. Pieroni, G. Ruggeri and F. Ciardelli, *Macromolecules*, 1995, **28**, 302–309.
33 O. Pieroni, A. Fissi, A. Viegi, D. Fabbri and F. Ciardelli, *J. Am. Chem. Soc.*, 1992, **114**, 2734–2736.
34 O. Pieroni, A. Fissi, J. L. Houben and F. Ciardelli, *J. Am. Chem. Soc.*, 1985, **107**, 2990–2991.
35 M. Sato, T. Kinoshita, A. Takizawa and Y. Tsujita, *Macromolecules*, 1988, **21**, 1612–1616.
36 M. Sisido, Y. Ishikawa, M. Harada and K. Itoh, *Macromolecules*, 1991, **24**, 3999–4003.
37 F. Ciardelli, D. Fabbri, O. Pieroni and A. Fissi, *J. Am. Chem. Soc.*, 1989, **111**, 3470–3472.
38 V. K. Kotharangannagari, A. Sanchez-Ferrer, J. Ruokolainen and R. Mezzenga, *Macromolecules*, 2011, **44**, 4569–4573.
39 O. Pieroni, A. Fissi and F. Ciardelli, *React. Funct. Polym.*, 1995, **26**, 185–199.
40 C. Y. Chen, Z. H. Wang and Z. B. Li, *Biomacromolecules*, 2011, **12**, 2859–2863.
41 J. T. Yan, K. Liu, X. Q. Zhang, W. Li and A. Zhang, *J. Polym. Sci., Part A: Polym. Chem.*, 2015, **53**, 33–41.
42 H. Lu and J. J. Cheng, *J. Am. Chem. Soc.*, 2007, **129**, 14114–14115.
43 H. Lu, Y. G. Bai, J. Wang, N. P. Gabrielson, F. Wang, Y. Lin and J. J. Cheng, *Macromolecules*, 2011, **44**, 6237–6240.
44 R. J. Dong, B. S. Zhu, Y. F. Zhou, D. Y. Yan and X. Y. Zhu, *Polym. Chem.*, 2013, **4**, 912–915.
45 R. Hu, N. L. C. Leung and B. Z. Tang, *Chem. Soc. Rev.*, 2014, **43**, 4494–4562.

